Switching polarity of oxidized detonation diamond nanoparticles on substrates

Stepan Stehlik, Tristan Petit, Hugues Girard, Jean-Charles Arnault, Alexander Kromka, Bohuslav Rezek

Switching polarity of oxidized detonation diamond nanoparticles on substrates

Stepan Stehlik [*,1], Tristan Petit [2], Hugues A. Girard [2], Jean-Charles Arnault [2], Alexander Kromka [1], Bohuslav Rezek [1]

[1] Institute of Physics ASCR, Cukrovarnická 10, 162 00, Prague 6, Czech Republic
[2] CEA, LIST, Diamond Sensors Laboratory, 91191 Gif-sur-Yvette, France
* Corresponding author: e-mail stehlik@fzu.cz, Phone: (+420) 220 318 475, Fax: (+420) 233 343 184

Abstract

Evaluation of diamond nanoparticles (DNPs) electrical potential under ambient environment is important for their application in electronics as well as sensors and biology. Here we use a novel methodology for characterization of nanoparticles based on recording of their electrical potential as a function of their size by two-pass Kelvin force microscopy (KFM). We study thermally oxidized detonation DNPs of 5 nm nominal size. The nanoparticles were deposited from diluted water solutions on a Si substrate half coated with Au. The KFM using conductive Si tip resolved characteristic negative potential differences of 10–60 mV on nanoparticles versus the substrate. When negative bias voltage to the KFM tip (−4 V) is applied during the topography acquisition (the first pass), subsequent potential measurement (the second pass) shows inversion of nanoparticles potential contrast. The same effects were observed also in the case of 20 nm colloidal Au nanoparticles. This effect is reversible and it is attributed to a charge retention in (or on) the nanoparticles.

Keywords diamond nanoparticles, gold nanoparticles, Kelvin force microscopy, surface charge, work function

1 Introduction

Diamond nanoparticles (DNPs) belong to family of nanomaterials where state of the surface (structure, electronic states, etc.) plays important role in the physical behavior of the material. Surface of diamond in the form of monocrystalline or a polycrystalline substrates can be desirably modified by plasma treatments [1], wet chemical treatments [2], annealing in vacuum or in air [3], organic chemistry [4], etc. The same holds for DNPs produced by detonation process [5], high pressure high temperature (HPHT) transformation and subsequent milling [6] or any other process leading to DNPs such as laser ablation [7]. Hydrogen surface terminations can be achieved by appropriate plasma treatment of DNPs and, as recently reported, hydrogenated DNPs (H-DNPs) still keep specific surface properties characteristic for hydrogen terminated diamond surface such as surface conductivity [8]. Oxidized DNPs (O-DNPs) are on the other hand insulators and their surface is terminated by various oxygen-containing groups (–OH, –COOH, –O–, etc.) [9]. Some preferences may be achieved by application of particular surface treatment (wet oxidation in acids [10], dry oxidation in oxygen plasma [11], or annealing in air [12]). Novel surface treatment is graphitization of DNPs surface by annealing in vacuum [13]. Depending on particular conditions one can obtain partially graphitized DNPs (G-DNPs) with distinct graphitic patches on their surfaces [14] or G-DNPs completely covered with few graphene layers and diamond core preserved underneath [15]. Complete graphitization of DNPs leads to nano-onions [16] which are promising due to their ability to store substantial charge for supercapacitors [17]. For the sake of completeness the fluorine and amino-group surface terminations have to be also mentioned [18]. These versatile initial surface modifications are then starting point to rich surface chemistry leading to diversely functionalized diamond surfaces for a broad field of applications [19].

Evaluation of DNPs electrical potential under ambient environment is important for their application in electronics as well as sensors and biology. Here, scanning probe microscopy methods such as

Kelvin force microscopy (KFM) become helpful as they enable mapping of electrical potentials with high spatial resolution. By measuring absolute value of contact potential difference between a probing tip and sample, work functions and electrostatic charges can be deduced. KFM is often denoted as surface potential measurement technique. However, KFM can detect and evaluate all potential changes that occur in the circuit, even inside the sample, such as photovoltages in the buried polypyrrole–diamond junction [20]. Moreover, also highly resistive materials can be characterized such as oxidized intrinsic diamond [21].

Because of its spatial resolution, KFM has been often used to characterize various nanoobjects including nanoparticles [22, 23], halide islands on metal substrates [24, 25], polymers [26], and nanostructured organic solar cells [27, 28]. This technique can be used even for investigation of localized charges and charge transfer on atomic scale [29-31]. We recently demonstrated that also electrical potential of DNPs with various surface terminations can be resolved. Apart from distinguishing subtle potential differences between H-DNPs, O-DNPs, and G-DNPs, inherent accommodation of DNPs potential according to the substrate material was observed [32]. In this paper, we demonstrate and explain switching polarity of the detonation DNPs (and gold nanoparticles as a reference system) on substrates in dependence on the applied bias voltage. We show that this directly evidences charging of the nanoparticles which was deduced in the previous study [32].

2 Experimental

We used detonation DNPs provided by the NanoCarbon Research Institute Co., Ltd. (Japan) with nominal size of 5 nm. The DNPs were annealed in air (4 h at 400 °C) to achieve oxidized surface [33]. Such O-DNPs were dispersed in water with help of sonication (Hielscher UP400S, 300 W, 24 kHz) for 2 h under cooling. The average nanoparticle size was ~10 nm as extracted from dynamic laser scattering technique [32]. From this colloidal solution the DNPs were then deposited on n-type Si wafers (10 Ω cm) with Au (20 nm) sputtered electrodes by drop-casting from a micropipette and letting dry in air afterwards. The concentration of the DNP dispersions was optimized to deposit scattered particles rather than continuous layers on the substrates.

Colloidal gold nanoparticles (GNPs) were used as a standard nanomaterial for comparison. We deposited 20 nm GNPs (BBI) on the above-mentioned Au–Si substrates. Adhesion of the GNPs towards Au–Si substrate was enhanced by addition of 1.2 µl of 5% HF to the 1 ml of the original colloidal solution [34]. The substrate was left in such prepared solution for 10 min to achieve proper coverage.

Kelvin force microscopy was performed by a scanning probe microscope (N-TEGRA system by NT-MDT) under ambient conditions (room temperature: 23–25 °C and relative humidity: 20–30%). Two-pass KFM technique with amplitude modulation was used. We used conductive silicon probes (Multi75Al-G, Budgetsensors) with high level of doping (0.01–0.025 Ω cm), with nominal tip radius of 10 nm and spring constant of 3 N m^{-1}. The set-point ratio was kept at 0.6 of the free oscillation amplitude (60 nm) in the first pass. The AC voltage in the second KFM pass was 5 V and the tip-sample distance offset was $\Delta z = 5$ nm. All the parameters were kept constant for all the KFM measurements. For the experiments with a biased tip +4 V or −4 V voltages were applied to the tip during the first pass. These voltages did not influence the topography signal.

3 Results

Figure 1 shows the AFM topography (a) together with corresponding KFM images (b–d) recorded after different bias voltage application. The AFM topography image indicates the presence of single O-DNPs as well as their aggregates up to ~35 nm size on the otherwise smooth Au substrate. It is visible from the KFM image obtained without applied bias (b) that the higher the nanoparticle or nanoparticle aggregate the higher its negative potential difference versus the substrate. This effect has been recently reported and discussed elsewhere [32]. When +4 V voltage to the tip during the first pass is applied the negative potential difference of the O-DNPs increases (Fig. 1c). On the other hand, the O-DNPs potential contrast turns to be positive versus Au substrate when negative −4 V voltage is applied on the tip during the first pass (Fig. 1d).

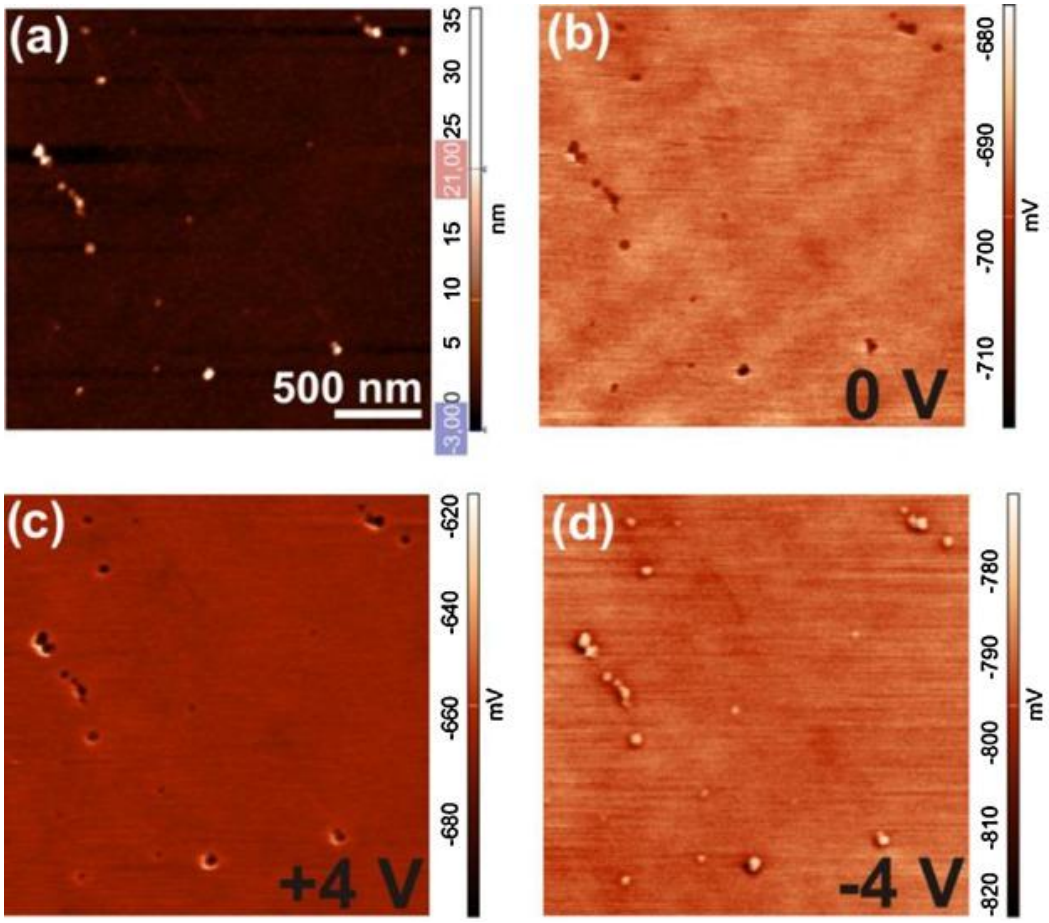

Figure 1. AFM topography image (a) of O-DNPs on Au substrate. Corresponding KFM images showing O-DNPs potential variations in dependence on the applied voltage and its polarity during the first pass: zero voltage (b), +4 V (c) and −4 V (d). Scan size 2.5 μm × 2.5 μm. Original *Z*-scale (35 nm) in topography image was slightly reduced (21 nm) to better visualize the smaller DNPs.

The potential dependences of the O-DNPs on their height are shown in the Fig. 2a. These data were extracted from the topography images (Fig. 1a) and corresponding KFM images at zero voltage (b), at +4 V (c) and −4 V (d). The data were linearly fitted based on the same procedure as in Ref. [32]. With zero applied voltage we observed a typical potential–height dependence with a negative slope [32]. When the positive voltage is applied to the tip during the first pass, the slope of the potential–height dependence becomes more negative. On the other hand, the slope of the dependence switches to positive when the negative voltage is applied. Note that the background potential, i.e., the potential of Au substrate slightly changes in dependence of the applied voltage polarity as well. This change is within ~180 mV. In order to clearly demonstrate the effect of the bias voltage we subtracted the

background potential of the Au substrate in accordance with our previously reported methodology [32]. The resulting data are plotted in Fig. 2b. The data show inversion of O-DNPs potential on Au substrate after application of −4 V. Similar data were obtained on Si substrate.

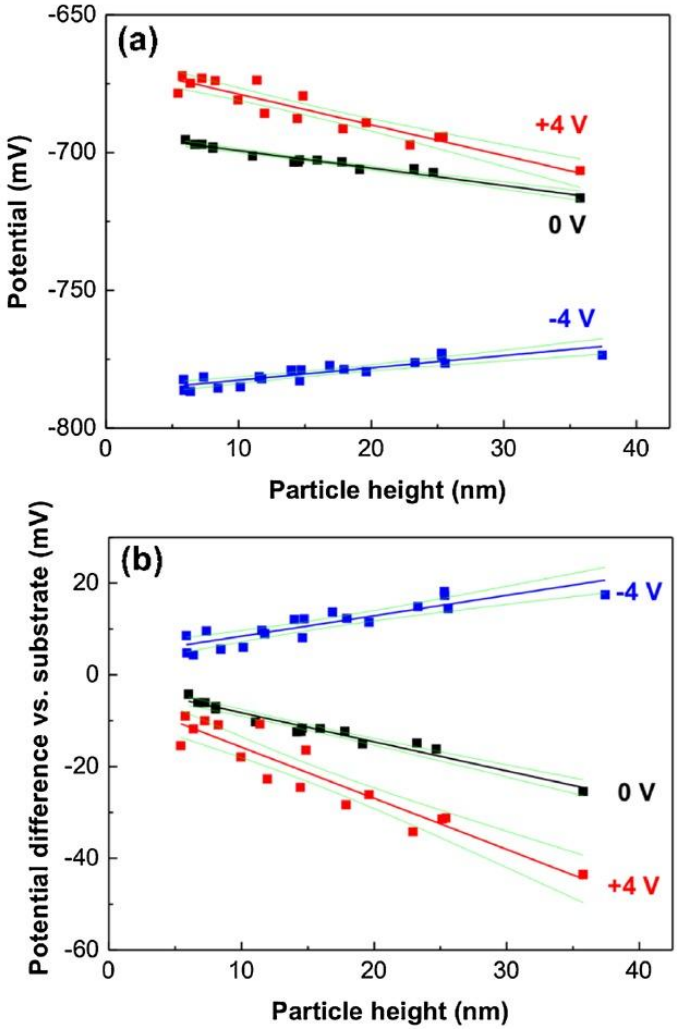

Figure 2. Potential values of O-DNPs on Au substrate in dependence on particle height as extracted from the Fig. 1. (a) Values of potential differences versus substrate in dependence on particle height with subtracted potential of the Au substrate. (b) The particular voltages are denoted as follows: +4 V red squares, 0 V black squares and −4 V blue squares. The lines correspond to a linear regression fit with 95% confidence bands.

The gold nanoparticles were found to behave in very similar way as DNPs in terms of accomodation of their potential to Au and Si substrates [32]. Thus, we employed them also to study the effect of the biased tip. For comparison, Fig. 3 the shows KFM image of 20 nm gold nanoparticles on Si substrate during changing the applied voltage to the tip in the sequence: 0, +4, −4, 0 V in direction from bottom to the top. The potential contrast of the Au nanoparticles versus the substrate changes in similar manner as in the case of O-DNPs. The potential of Au nanoparticles becomes more negative when +4 V voltage is applied. The contrast inverts when −4 V voltage is applied, i.e., the Au nanoparticle potential becomes positive versus the substrate. After the bias is turned off the potential difference versus substrate returns to its original value. It is important to mention that the inversion and recovery of the potential contrast is rather slow process in the order of 10 s.

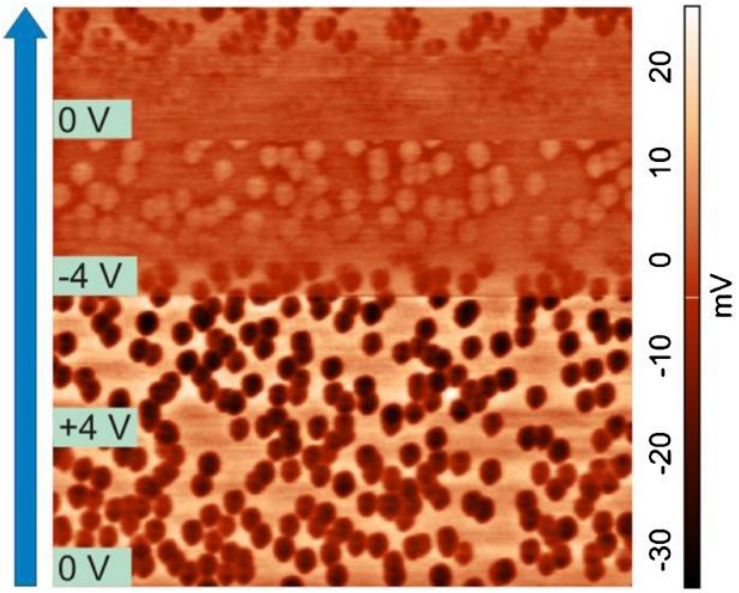

Figure 3. KFM image of 20 nm Au nanoparticles upon changing of applied voltage to the tip during the first pass, slow scan direction upwards, scan size 2 μm × 2 μm. The applied voltages are indicated at the left-hand side of the image. The background potential of the Si substrate was subtracted for better visualization of the potential contrast changes.

4 Discussion

Relative comparison of KFM potentials recorded on sample should generally not depend on the tip material or polarity. Nevertheless, Yurtsever et al. [35] recently reported the tip-polarity-dependent contrast inversion in local contact potential difference signal of Ca^{2+} and F^{-} ions of CaF_2 thin films in UHV atomically resolved AFM/KFM. Although we cannot directly compare the atomically resolved AFM/KFM images obtained at ultra-high vacuum conditions with our results obtained at ambient conditions some parallels can be still made. Two mechanisms to explain the contrast variations may by proposed. (i) charge transfer between the tip and sample (nanoparticle or single ion), (ii) polarization effects at the tip-surface interface. In our ambient conditions the situation is further complicated by a thin water adsorbate layer [36] which may contribute to both of the proposed mechanisms.

As for possible nanoparticle polarization, on GNP the polarization dissipates much faster (incl. surfactants) compared to the speed of KFM measurement (1 s from 1 side of image to the other side + another 1 s from charging in first-pass). Also the time constant of polarization of adsorbed water and water ion molecules on the surface is typically in the order of 0.1 s or less. Therefore, the observed and comparable potential difference on diamond and gold nanoparticles after bias voltage application must be mostly due to retention of electrostatic charge in or on the nanoparticles. Nevertheless, the potential of Au electrode should remain constant as the bias voltages are applied only during the 1st pass, not during the potential measurement itself. Thus, overall shifts of the potential in Fig. 2a must be due to charging of the Si tip during the 1st pass. As the Si AFM tips are highly doped the charge may be localized in the native oxide on the tip surface. The temporary nature of this effect was verified by subsequent ordinary KFM scan (0 V in the first pass) of the same spot. Similar KFM image and potential values of the Au substrate as well as of the nanoparticles were observed as in the case of Fig. 1b. Thus we can exclude a non-reversible change of the tip by voltage-induced effects; i.e., anodic oxidation.

Positive bias voltage and hence charge or polarization on the tip can be understood as an increase in the tip work function. Consequently the contact potential difference of the Si tip with the substrate should become less negative [37] and vice versa for the negative bias voltage. This is exactly observed

in Fig. 2a. The offsets are not the same and also do not correspond to 4 V, because the induced potential difference is obviously typically much smaller than the applied voltage [38], the bias voltage adds or subtracts from initial contact potential difference, and there may be also additional potential drops in the circuit.

Considering possible charging of the tip (and thus apparent change of work function) the different charging of the nanoparticles could be merely due to change of contact potential difference between the tip and substrate which leads to different amount and polarity of transferred charge. Then the relative potential difference versus substrate in Fig. 2b should follow the same trend as in Fig. 2a, i.e., nanoparticles should become less negative after the +4 V bias voltage application. However, the opposite effect is observed. This can be understood if we consider that positive potential on the tip means negative potential on the substrate. Thus the observed contrast means that the nanoparticles retain some of the negative charge from the Au substrate even after the voltage is switched off during 2nd pass of KFM measurement. This is unlike the situation with real high work function tip (such as Pt coated tips) where after connection with the substrate of lower work function some electrons will flow to the tip and the substrate becomes charged positively. The above observation also indicates that the charge is transferred from substrate rather than from the tip. This is understandable as there is a gap or only a weak contact in the semicontact regime in which KFM is operated. Thus, the intentional charging applied here helps resolve some of the questions remaining in the previous study [32]. In principle, the opposite charging polarity than expected could be also due to the change of DNP surface work function by change of energetic band bending in the semiconductor materials. This effect has been observed previously on amorphous silicon thin films [39]. However, here we observe similar effect on gold nanoparticles which are metallic. Thus the effect must be attributed to electrostatic charging as explained above.

5 Conclusions

We showed inversion of potential contrast of diamond and gold nanoparticles on Au and Si substrates in dependence on the tip voltage and polarity. Using conductive silicon tip we observed a negative potential of the nanoparticles versus any of the substrates in two-pass KFM technique. When we applied +4 V to the tip during the first pass (topography measurement) the contrast in the second pass (potential measurement) became more negative. Inversion to positive contrast occurred when −4 V bias was applied. If we consider that positive potential on the tip means negative potential on the substrate and that the delay between the first and second pass measurement on one spot is about 2 s, the nanoparticles must obviously retain some of the negative charge from the substrate. It works similarly on the Si substrate. This effect is reversible and it directly evidences inherent as well as intentional electrostatic charging of both O-DNPs and Au nanoparticles from substrates where other effects such as polarization play negligible role. This corroborates our recently proposed model how nanoparticles assume their potential according to their size, surface modification, and substrate they reside on [32] and it may also provide insight for understanding phenomena influenced by electrical potentials of the nanoparticles in general.

Acknowledgements

Technical support by Jitka Libertínová and Martin Müller is gratefully appreciated. Authors thank Prof. E. Osawa for providing DNPs. This research was financially supported by the projects P108/12/G108 (GACR). This work occurred in frame of the LNSM infrastructure.

References

[1] H. Kawarada, *Surf. Sci. Rep.* **26**, 207 (1996).

[2] H. Kozak, A. Kromka, E. Ukraintsev, J. Zemek, M. Ledinský, M. Vaněček, B. Rezek, *Diam. Relat. Mater.* **18**, 722–725 (2009).

[3] J. Ristein, *Surf. Sci.* **600**, 3677–3689 (2006).

[4] B. Rezek, D. Shin, H. Uetsuka, C. E. Nebel, *Phys. Status Solidi A* **204**, 2888–2897 (2007).

[5] P. J. De Carli, J. C. Jameieson, *Science* **133**, 1821–1822 (1961).

[6] J. P. Boudou, P. A. Curmi, F. Jelezko, J. Wrachtrup, P. Aubert, M. Sennour, G. Balasubramanian, R. Reuter, A. Thorel, E. Gaffet, *Nanotechnology* **20**, 235602 (2009).

[7] G. W. Yang, J. B. Wang, Q. X. Liu, *J. Phys.: Condens. Matter* **10**, 7923–7927 (1998).

[8] H. A. Girard, T. Petit, S. Perruchas, T. Gascoin, C. Gesset, J. C. Arnault, P. Bergonzo, *Phys. Chem. Chem. Phys.* **13**, 11517–11523 (2011).

[9] V. N. Mochalin, O. Shenderova, D. Ho, Y. Gogotsi, *Nature Nanotechnol.* **7**, 11–23 (2012).

[10] V. Y. Dolmatov, *Usp. Khim.* **70**, 687–708 (2001).

[11] H. Kozak, Z. Remes, J. Houdkova, S. Stehlik, A. Kromka, B. Rezek, *J. Nanopart. Res.* **15**, 1568 (2013).

[12] O. Shenderova et al., *Diam. Relat. Mater.* **15**, 1799–1803 (2006).

[13] J. Chen, S. Z. Deng, J. Chen, Z. X. Yu, N. S. Xu, *Appl. Phys. Lett.* **74**, 3651 (1999).

[14] T. Petit, J.-C. Arnault, H. A. Girard, M. Sennour, T.-Y. Kang, C.-L. Cheng, P. Bergonzo, *Nanoscale* **4**, 6792 (2012).

[15] Z. Qiao, J. Li, N. Zhao, Ch. Shi, P. Nash, *Scripta Mater.* **54**, 225–2229 (2006).

[16] F. Banhart, P. M. Ajayan, *Nature* **382**, 433–435 (1996).

[17] D. Pech, M. Brunet, H. Durou, P. Huang, V. Mochalin, Y. Gogotsi, P. L. Taberna, P. Simon, *Nature Nanotechnol.* **5**, 651–654 (2010).

[18] Y. Liu, Z. N. Gu, J. L. Margrave, V. N. Khabashesku, *Chem. Mater.* **16**, 3924–3930 (2004).

[19] A. Krueger, D. Lang, *Adv. Func. Mater.* **22**, 890–906 (2012).

[20] B. Rezek, J. Čermák, A. Kromka, M. Ledinský, J. Kočka, *Diam. Relat. Mater.* **18**, 249–252 (2009).

[21] B. Rezek, C. E. Nebel, *Diam. Relat. Mater.* **14**, 466–469 (2005).

[22] M. A. Salem, H. Mizuta, S. Oda, *Appl. Phys. Lett.* **85**, 3262 (2004).

[23] T. Yamauchi, M. Tabuchi, A. Nakamura, *Appl. Phys. Lett.* **84**, 3834 (2004).

[24] C. Loppacher, U. Zerweck, L. M. Eng, *Nanotechnology* **15**, S9–S13 (2004).

[25] Th. Glatzel, L. Zimmerli, S. Koch, B. Scuh, S. Kawai, E. Meyer, *Nanotechnology* **20**, 264016 (2009).

[26] S. Magonov, J. Alexander, *Beilstein J. Nanotechnol.* **2**, 15–27 (2011).

[27] E. J. Spadafora, R. Demadrille, B. Ratier, B. Grévin, *Nano Lett.* **10**, 3337–3342 (2010).

[28] J. Čermák, B. Rezek, V. Cimrová, D. Výprachtický, M. Ledinský, T. Mates, A. Fejfar, J. Kočka, *Phys. Status Solidi RRL* **1**, 193–195 (2007).

[29] F. Mohn, L. Gross, N. Moll, G. Meyer, *Nature Nanotechnol.* **7**, 227–231 (2012).

[30] T. Hynninen, S. A. Foster, *e-J. Surf. Sci. Nanotechnol.* **9**, 6–14 (2011).

[31] S. Sadewasser, P. Jelinek, Ch.-K. Fang, O. Custance, Y. Yamada, Y. Sugimoto, M. Abe, S. Morita, *Phys. Rev. Lett.* **103**, 266103 (2009).

[32] S. Stehlik, T. Petit, H. A. Girard, J.-C. Arnault, A. Kromka, B. Rezek, *Langmuir* **29**, 1634 (2013).

[33] S. Osswald, G. Yushin, V. Mochalin, S. O. Kucheyev, Y. Gogotsi, *J. Am. Chem. Soc.* **128**, 11635–11642 (2006).

[34] M. Kolíbal, M. Konečný, F. Ligmajer, D. Škoda, T. Vystavěl, J. Zlámal, P. Varga, T. Šikola, *ACS Nano* **6**, 10098–10106 (2012).

[35] A. Yurtsever, Y. Sugimoto, M. Fukumoto, M. Abe, S. Morita, *Appl. Phys. Lett.* **101**, 083119 (2012).

[36] H. Sugimura, Y. Ishida, K. Hayashi, O. Takai, N. Nakagiri, *Appl. Phys. Lett.* **80**, 1459 (2002).

[37] B. Rezek, C. Sauerer, C. E. Nebel, M. Stutzmann, J. Ristein, L. Ley, E. Snidero, P. Bergonzo, *Appl. Phys. Lett.* **82**, 2266–2268 (2003).

[38] E. Verveniotis, A. Kromka, M. Ledinský, B. Rezek, *Diam. Relat. Mater.* **24**, 39–43 (2012).

[39] B. Rezek, T. Mates, J. Stuchlík, J. Kočka, A. Stemmer, *Appl. Phys. Lett.* **83**, 1764–1766 (2003).